# A Convex Approach for Image Restoration with Exact Poisson-Gaussian Likelihood

Anna Jezierska, Emilie Chouzenoux, Jean-Christophe Pesquet, Hugues Talbot

# A Convex Approach for Image Restoration with Exact Poisson-Gaussian Likelihood

Anna Jezierska, *Member, IEEE*, Emilie Chouzenoux, *Member, IEEE*, Jean-Christophe Pesquet, *Fellow, IEEE*, Hugues Talbot, *Member, IEEE*

***Abstract*—The Poisson-Gaussian model can accurately describe the noise present in a number of imaging systems. However most existing restoration methods rely on approximations of the Poisson-Gaussian noise statistics. We propose a convex optimization strategy for the reconstruction of images degraded by a linear operator and corrupted with a mixed Poisson-Gaussian noise. The originality of our approach consists of considering the exact, mixed continuous-discrete model corresponding to the data statistics. After establishing the Lipschitz differentiability and convexity of the Poisson-Gaussian neg-log-likelihood, we derive a primal-dual iterative scheme for minimizing the associated penalized criterion. The proposed method is applicable to a large choice of convex penalty terms. The robustness of our scheme allows us to handle computational difficulties due to infinite sums arising from the computation of the gradient of the criterion. We propose finite bounds for these sums, that are dependent on the current image estimate, and thus adapted to each iteration of our algorithm. The proposed approach is validated on image restoration examples. Then, the exact data fidelity term is used as a reference for studying some of its various approximations. We show that in a variational framework the Shifted Poisson and Exponential approximations lead to very good restoration results.**

***Index Terms*—Poisson-Gaussian noise, convex optimization, proximal methods, primal-dual algorithm, image restoration**

## I. Introduction

The recovery of a target image in the presence of degradations (i.e. noise) has been widely studied in the literature. Image reconstruction problems are often formulated into the Maximum *A Posteriori* (MAP) framework. The MAP estimator is computationally simple and offers significant flexibility in the choice of a prior, while the data fidelity term usually consists of the noise neg-log-likelihood or some approximation. A Gaussian noise model is commonly assumed in imaging due to the simple and intuitive form of the related data fidelity function, which is strongly convex and Lipschitz differentiable. However, recent methodological progress has ensured that more sophisticated estimation problems can be efficiently solved numerically. As a consequence, studies are no longer limited to the simplest Gaussian case. Some contributions concern various standard noise distributions, e.g. Poisson [2], [3], [4], [5], [6], impulsive [7] or multiplicative [8] noise, as well as some mixed noise models, e.g. the mixture of Gaussian and impulsive noise [9], [10].

A growing interest in Poisson-Gaussian probabilistic models has recently been observed. The Poisson component is often related to the quantum nature of light and accounts for photon-counting principles in signal acquisition, whereas the Gaussian component is typically related to noise present in the electronic part of the imaging system. Despite constant improvements, electronic noise usually cannot be neglected. As a consequence, Poisson-Gaussian noise is frequently encountered in astronomy [11], [12], medicine [13] and biology [14]. There has been a growing interest for denoising problems involving images corrupted in this fashion [15], [16], [17]. However, the literature involving this model in deconvolution and reconstruction problems remains scarce. Among existing works, Benvenuto *et al.* [11] proposed a scaled gradient method and more recently Gil-Rodrigo *et al.* [18] developed an alternating minimization algorithm. An augmented Lagrangian method grounded on a Poisson approximation of the noise characteristics was proposed in [19], while a similar framework with a weighted squared $\ell_2$ norm noise approximation was proposed in [20]. So far, restoration strategies have relied on some approximations of the noise statistics, which may have been detrimental to the quality of the results. The use of approximations is motivated by the mathematical difficulties raised by the Poisson-Gaussian model. Indeed, the corresponding probability distribution has a discrete-continuous nature, and the expression of the associated log-likelihood function involves infinite sums. For simplification, one usually neglects either the Poisson or the Gaussian component, or performs an approximation of the Poisson-Gaussian model based on variance stabilization techniques [21], [22].

In this paper, we investigate the properties of the Poisson-Gaussian negative log-likelihood, showing that it is a convex Lipschitz differentiable function. Since the gradient of the Poisson-Gaussian neg-log-likelihood requires the computation of infinite series, we propose to employ proximal optimization methods whose convergence is guaranteed even in the presence of summable numerical errors. Among recent approaches, only a few splitting algorithms [23], [24], [25], [26] can cope with the sum of a gradient Lipschitz term and possibly nonsmooth penalty terms. Such terms can model a wide range of prior information, e.g. range value constraints, criteria promoting sparsity in a frame, total-variation and more generally hybrid regularization functions [27].

The paper is organized as follows: Section II introduces the notation used in this work and investigates the Poisson-

Part of this work appeared in the conference proceedings of ICASSP, 2012 [1]. This work was supported by the Agence Nationale de la Recherche under grant ANR-09-EMER-004-03.

A. Jezierska, E. Chouzenoux (Corresponding Author), J.-C. Pesquet and H. Talbot are with the Université Paris-Est, Laboratoire d'Informatique Gaspard Monge, CNRS-UMR 8049, 77454 Marne-la-Vallée Cedex 2, France. Phone: +33 1 60 95 72 88, E-mail: {first.last}@univ-mlv.fr.

Gaussian model. In particular, convexity and Lipschitz-differentiability results are presented. Section III describes the proposed optimization framework. Next, various approximation strategies are compared and our approach is illustrated via experiments in Section IV. Finally, some conclusions are drawn in Section V.

## II. Degradation model

Let $y = (y_i)_{1\leq i\leq Q} \in \mathbb{R}^Q$ be a vector of observations related to an original signal $\overline{x} \in [0,+\infty)^N$, which is degraded by a matrix $H$ in $[0,+\infty)^{Q\times N}$ (e.g., a convolutive model) and further corrupted with Poisson-Gaussian noise. More specifically, the observations $y$ are related to $\overline{x}$ by

$$y = z(\overline{x}) + w, \tag{1}$$

where $z(\overline{x}) = \big(z_i(\overline{x})\big)_{1\leq i\leq Q}$ and $w = (w_i)_{1\leq i\leq Q}$ are realizations of mutually independent random vectors $Z(\overline{x}) = \big(Z_i(\overline{x})\big)_{1\leq i\leq Q}$ and $W = (W_i)_{1\leq i\leq Q}$ featuring independent components. It is further assumed that, for every $i \in \{1,\ldots,Q\}$,

$$Z_i(\overline{x}) \sim \mathcal{P}([H\overline{x}]_i), \tag{2}$$

$$W_i \sim \mathcal{N}(0,\sigma^2), \tag{3}$$

where $[H\overline{x}]_i$ is the $i$-th component of vector $H\overline{x}$, and $\sigma \in (0,+\infty)$ is the standard deviation of the zero-mean Gaussian noise component. Hence, $y$ is a realization of a random vector $Y$ with probability density function

$$p_{Y|\overline{x}}(y) = \prod_{i=1}^{Q}\left(\sum_{n=0}^{+\infty}\frac{e^{-[H\overline{x}]_i}([H\overline{x}]_i)^n}{n!}\frac{e^{-\left(\frac{y_i-n}{\sqrt{2}\sigma}\right)^2}}{\sqrt{2\pi}\sigma}\right). \tag{4}$$

In the context of inverse problems, the original signal can be recovered by minimizing a penalized criterion:

$$\min_{x\in\mathbb{R}^N}\left(f(x) = \Phi(x) + \rho(x)\right), \tag{5}$$

where $\Phi$ is the so-called data fidelity term and $\rho$ is a regularization function incorporating *a priori* information, so as to guarantee the stability of the solution w.r.t. the observation noise. In the Bayesian framework, this allows us to compute the MAP estimate [28] of the original image. In this context, the data fidelity term is defined as the negative logarithm of $p_{Y|x}(y)$:

$$\Phi(x) = -\log(p_{Y|x}(y)) = \sum_{i=1}^{Q}\Phi_i([Hx]_i), \tag{6}$$

where, for every $i \in \{1,\ldots,Q\}$ and $u \in [0,+\infty)$,

$$\Phi_i(u) = -\log\left(\sum_{n=0}^{+\infty}\frac{u^n e^{-u}}{n!}\frac{e^{-\left(\frac{y_i-n}{\sqrt{2}\sigma}\right)^2}}{\sqrt{2\pi}\sigma}\right), \tag{7}$$

and the regularization term $\rho$ corresponds to the potential of the chosen prior probability density function of the target image.

Let $\mathbb{1}$ denote the vector of $\mathbb{R}^Q$ with all its components equal to 1. The gradient and Hessian of $\Phi$ on the positive orthant are respectively given by: for every $x \in [0,+\infty)^N$,

$$\nabla\Phi(x) = H^\top(\mathbb{1} - \xi(Hx)), \tag{8}$$

$$\nabla^2\Phi(x) = H^\top \mathrm{Diag}\left(\eta_1([Hx]_1),\ldots,\eta_Q([Hx]_Q)\right)H, \tag{9}$$

where, for every $z = (z_i)_{1\leq i\leq Q} \in [0,+\infty)^Q$, $\xi(z) = \big(\xi_i(z_i)\big)_{1\leq i\leq Q}$, $\eta(z) = \big(\eta_i(z_i)\big)_{1\leq i\leq Q}$ with

$$\xi_i(z_i) = s(z_i, y_i-1)/s(z_i,y_i), \tag{10}$$

$$\eta_i(z_i) = \big(s(z_i,y_i-1)^2 - s(z_i,y_i)s(z_i,y_i-2)\big)/s(z_i,y_i)^2, \tag{11}$$

and, for every $(a,b) \in \mathbb{R}^2$,

$$s(a,b) = \sum_{n=0}^{+\infty}\frac{a^n}{n!}e^{-\left(\frac{b-n}{\sqrt{2}\sigma}\right)^2}. \tag{12}$$

A common, useful technique for solving large-size optimization problems such as those encountered in image recovery consists of splitting (i.e. decomposing) the cost function $f$ in a sum of simpler functions, which are then processed individually. For example, each of these functions can be dealt with through its gradient if the function is $\mu$-Lipschitz differentiable[1], or through its proximity operator [30], [31] if the latter has a closed form expression.

In view of this, the two following results are essential to our approach.

**Theorem II.1** *The function $\Phi$ is $\mu$-Lipschitz differentiable on $[0,+\infty)^N$ with*

$$\mu = \|H\|^2\left(1 - e^{-\frac{1}{\sigma^2}}\right) \times \exp\left(\frac{1}{\sigma^2}\left(2\max_{i\in\{1,\ldots,Q\}}\{y_i\} - 1\right)\right). \tag{13}$$

*Proof:* See Appendix A ∎

The next convexity result can be regarded as an extension to the one presented in [11].

**Theorem II.2** *The neg-log-likelihood $\Phi^{(\beta)}$ of a mixture of Generalized-Gaussian and Poisson variables defined over the positive orthant as*

$$\big(\forall x \in [0,+\infty)^N\big)\quad \Phi^{(\beta)}(x) = \sum_{i=1}^{Q}\Phi_i^{(\beta)}([Hx]_i) \tag{14}$$

*where, for every $i \in \{1,\ldots,Q\}$ and $u \in [0,+\infty)$,*

$$\Phi_i^{(\beta)}(u) = -\log\left(\sum_{n=0}^{+\infty}\frac{u^n e^{-u}}{n!}\frac{\beta}{2\sqrt{2}\sigma\Gamma(\frac{1}{\beta})}e^{-\left(\frac{|y_i-n|}{\sqrt{2}\sigma}\right)^\beta}\right) \tag{15}$$

*is convex if $\beta \geq 1$. It is strictly convex if $\beta > 1$ and $H$ is injective.*

*Proof:* See Appendix B ∎

Some convex Lipschitz differentiable approximations of the data fidelity term (6) and of its gradient (8) proposed in various works concerning Poisson-Gaussian data restoration are summarized in Table I.

[1] A differentiable function $f : \mathbb{R}^N \to \mathbb{R}$ is said to be $\mu$-Lipschitz differentiable on a subset $C \subset \mathbb{R}^N$ if its gradient $\nabla f$ is such that, for every $(x,y) \in C^2$, $\|\nabla f(x) - \nabla f(y)\| \leq \mu\|x-y\|$.

| Name | Expression | Convexity condition | Lipschitz constant |
|---|---|---|---|
| Generalized Anscombe Transform (GAST) [21] | $\widetilde{\Phi}_i(u) = \frac{1}{2}\left(\nu(y_i) - \nu(u)\right)^2$, $\widetilde{\xi}_i(u) = \frac{2\nu(y_i)}{\nu(u)} - 1$ with $\nu(u) = 2\sqrt{u + 3/8 + \sigma^2}$ | $y_i + 3/8 + \sigma^2 \geq 0$ | $\mu_i = (3/8 + \sigma^2)^{-3/2}\frac{\nu(y_i)}{2}$ |
| Exponential (EXP) [11] | $\widetilde{\Phi}_i(u) = u - \frac{1/2 - y_i - \sigma^2}{e}\mathrm{Ei}\left(\frac{\sigma^2 - 1/2 + y_i}{\sigma^2 + u}\right) - (\sigma^2 + u)e^{-\frac{1/2 - y_i + u}{\sigma^2 + u}}$, $\widetilde{\xi}_i(u) = \exp\left(-\frac{1 + 2u - 2y_i}{2u + 2\sigma^2}\right)$ | $y_i + \sigma^2 - 1/2 \geq 0$ | $\mu_i = \frac{2y_i + 2\sigma^2 - 1}{2\sigma^4}\exp\left(\frac{2y_i - 1}{2\sigma^2}\right)$ |
| Shifted Poisson (SPoiss) [19] | $\widetilde{\Phi}_i(u) = \eta(u) - \eta(y_i)\log\eta(u)$, $\widetilde{\xi}_i(u) = \frac{\eta(y_i)}{\eta(u)}$ with $\eta(u) = u + \sigma^2$ | $y_i + \sigma^2 \geq 0$ | $\mu_i = \frac{y_i + \sigma^2}{\sigma^4}$ |
| Weighted least squares (WL2) [11], [18], [20], [29] | $\widetilde{\Phi}_i(u) = \frac{1}{2}\frac{(y_i - u)^2}{\sigma^2 + u}$, $\widetilde{\xi}_i(u) = \frac{(y_i + \sigma^2)^2}{4(u + \sigma^2)^2} + \frac{3}{4}$ | — | $\mu_i = \frac{(y_i + \sigma^2)^2}{\sigma^6}$ |

TABLE I

VARIOUS APPROXIMATIONS $\widetilde{\Phi}(x) = \sum_{i=1}^{Q}\widetilde{\Phi}_i([Hx]_i)$ (UP TO AN ADDITIVE CONSTANT) OF THE POISSON-GAUSSIAN NEG-LOG-LIKELIHOOD $\Phi(x)$, TOGETHER WITH THEIR GRADIENT $\nabla\widetilde{\Phi}(x) = H^\top(\mathbb{1} - (\widetilde{\xi}_i([Hx]_i)_{1\leq i\leq Q})$. EI DENOTES THE EXPONENTIAL INTEGRAL FUNCTION. WE PROVIDE THE CONDITIONS ON $y$ FOR $\widetilde{\Phi}$ TO BE CONVEX AND THE EXPRESSION OF THE LIPSCHITZ CONSTANT $\mu = \|H\|^2\max_{i\in\{1,\dots,Q\}}\mu_i$ OF $\nabla\widetilde{\Phi}$.

For the optimization methods developed in the next section, it is also important to note that the definition of the negative log-likelihood (6) can be extended to the whole space $\mathbb{R}^N$ by setting, for every $x \in \mathbb{R}^N$,

$$\Phi(x) = h(x) + \iota_{[0,+\infty)^N}(x), \tag{16}$$

where

$$h(x) = \sum_{i=1}^{Q}\varphi_i([Hx]_i), \tag{17}$$

$$\iota_{[0,+\infty)^N}(x) = \begin{cases} 0 & \text{if } x \in [0,+\infty)^N, \\ +\infty & \text{otherwise.} \end{cases} \tag{18}$$

For every $i \in \{1,\dots,Q\}$, the function $\varphi_i$ is a convex, twice-differentiable function, whose expression is given by

$$\varphi_i\colon \mathbb{R} \to \mathbb{R}$$
$$u \mapsto \begin{cases} \Phi_i(u) & \text{if } u \in [0,+\infty], \\ \frac{1}{2}\eta_i(0)u^2 + (1 - \xi_i(0))u + \Phi_i(0) & \text{otherwise,} \end{cases} \tag{19}$$

where functions $\Phi_i$, $\xi_i$ and $\eta_i$ are defined in (7), (10) and (11) respectively. We note that for $a = 0$ the infinite sum (12) simplifies to the first sum term, i.e. $s(0,b) = e^{-\frac{b^2}{2\sigma^2}}$. Hence, for every $i \in \{1,\dots,Q\}$, the expressions of $\xi_i(0)$ and $\eta_i(0)$ in (19) read

$$\xi_i(0) = e^{\frac{1}{2\sigma^2}(2y_i - 1)}, \tag{20}$$

$$\eta_i(0) = \left(1 - e^{-\frac{1}{\sigma^2}}\right)e^{\frac{1}{\sigma^2}(2y_i - 1)}. \tag{21}$$

Consequently, $h$ is a convex function with a $\mu$-Lipschitz gradient on $\mathbb{R}^N$. The positivity constraint in the original problem is imposed by the indicator function (18).

## III. PROPOSED OPTIMIZATION METHOD

### A. Minimization problem

According to the analysis carried out in Section II, the objective function has the following form

$$(\forall x \in \mathbb{R}^N) \quad f(x) = h(x) + \psi_0(x) + \sum_{r=1}^{R}\psi_r(V_r x), \tag{22}$$

where the regularization term is split into a sum of simpler functions. More precisely, it will be assumed that $\psi_0 \in \Gamma_0(\mathbb{R}^N)$ and, for every $r \in \{1,\dots,R\}$, $\psi_r \in \Gamma_0(\mathbb{R}^{P_r})$ and $V_r \in \mathbb{R}^{P_r\times N}$.[2] Note that (22) covers a large range of penalization strategies. For instance, a sparsity prior in an analysis frame with frame operator $V_r$ is introduced by taking $\psi_r$ equal to $\lambda_r\|\cdot\|_1$ with $\lambda_r > 0$ [33]. Block sparsity measures [34] can also be easily addressed in the proposed framework. Another popular example in image restoration is the total variation penalization [35].[3] In this case, $P_r = 2N$, $V_r = \left[(\Delta^{\mathrm{h}})^\top\ (\Delta^{\mathrm{v}})^\top\right]^\top$, where $\Delta^{\mathrm{h}} \in \mathbb{R}^{N\times N}$ (resp. $\Delta^{\mathrm{v}} \in \mathbb{R}^{N\times N}$) corresponds to a horizontal (resp. vertical) gradient operator, and, for every $x \in \mathbb{R}^N$, $\psi_r(V_r x) = \lambda_r\sum_{n=1}^{N}\left(([\Delta^{\mathrm{h}}x]_n)^2 + ([\Delta^{\mathrm{v}}x]_n)^2\right)^{1/2}$ with $\lambda_r > 0$. Another

[2]Following standard notation in convex analysis [32], $\Gamma_0(\mathbb{R}^N)$ designates the class of lower-semicontinuous, proper, convex functions from $\mathbb{R}^N$ to $(-\infty,+\infty]$.

[3]Total variation and the Hessian-based penalization correspond to improper priors.

interesting choice is the Hessian-based penalization [36], [37] i.e., $P_r = 3N$ and $V_r = [\left(\Delta^{\mathrm{hh}}\right)^\top \ \sqrt{2}\left(\Delta^{\mathrm{hv}}\right)^\top \ \left(\Delta^{\mathrm{vv}}\right)^\top]^\top$ where $\Delta^{\mathrm{hh}} \in \mathbb{R}^{N\times N}$, $\Delta^{\mathrm{hv}} \in \mathbb{R}^{N\times N}$ and $\Delta^{\mathrm{vv}} \in \mathbb{R}^{N\times N}$ model the second-order partial finite difference operators between neighbooring pixels as described in [37, Sec.III-A] and, for every $x \in \mathbb{R}^N$, $\psi_r(V_r x) = \lambda_r \sum_{n=1}^N \left(([\Delta^{\mathrm{hh}} x]_n)^2 + 2([\Delta^{\mathrm{hv}} x]_n)^2 + ([\Delta^{\mathrm{vv}} x]_n)^2\right)^{1/2}$ with $\lambda_r > 0$. The above penalties can be considered individually ($R = 1$) or combined in a hybrid manner ($R > 1$) [27]. Finally, following (16), $\psi_0$ should be the indicator function $\iota_{[0,+\infty)^N}$. However, to take into account the dynamic range of the expected output image, it can be more generally chosen equal to the indicator function $\iota_C$ of a nonempty closed convex subset $C$ of $[0,+\infty)^N$.

### B. Primal-dual splitting algorithm

Problem (5) where $f$ takes the form (22) can be efficiently addressed using proximal splitting algorithms [23], [24], [38], [39]. The solution is obtained iteratively by evaluating the individual proximity operators of the functions $(\psi_r)_{0\leq r\leq R}$, provided that they have an explicit expression. We first require the notion of proximity operator.

**Definition III.1** [30], [31] *The value at $x \in \mathbb{R}^N$ of the proximity operator of a function $f \in \Gamma_0(\mathbb{R}^N)$, denoted by $\mathrm{prox}_f : \mathbb{R}^N \mapsto \mathbb{R}^N$, is the unique solution to the following minimization problem:*

$$(\forall x \in \mathbb{R}^N) \quad \mathrm{prox}_f(x) := \operatorname*{argmin}_{p\in\mathbb{R}^N} f(p) + \frac{1}{2}\|x-p\|^2. \quad (23)$$

The proximity operator is firmly nonexpansive, i.e. for every $(x,x') \in \mathbb{R}^N \times \mathbb{R}^N$,

$$\left(\mathrm{prox}_f(x) - \mathrm{prox}_f(x')\right)^\top (x-x') \geq \left\|\mathrm{prox}_f(x) - \mathrm{prox}_f(x')\right\|^2 \quad (24)$$

and its fixed points are the minimizers of function $f$. Numerous convex optimization algorithms are based on this concept (see [40], [41] for tutorials) due to these properties. In the context of the minimization of (22), we are interested in algorithms which incorporate functions $h$ and $(\psi_r)_{0\leq r\leq R}$ either via their proximity operators or via their gradients. The presence of a smooth term is of paramount important as we have shown our data fidelity term $h$ to be $\mu$-Lipschitz differentiable, while its proximity operator does not have a closed form expression. Note that not all proximal methods offer the required flexibility to address the minimization of (22). More precisely, in the case when $R = 0$, one can employ either the forward-backward (FB) [42] [43, Chapter 3] or the forward-backward-forward (FBF) algorithms [44]. Conversely, celebrated algorithms such as Douglas-Rachford's [45], [46] or the Alternating Direction Method of Multipliers [35], [47], [48], would be difficult to implement. In the case when $R \neq 0$, one can resort to primal-dual techniques proposed in [23], [49] and [26], [25][4] which can be regarded as extensions of the FBF and FB algorithms, respectively.

[4]The latter algorithms are generalizations of the primal-dual technique developed in [50].

We are now ready to present our primal-dual splitting algorithm. The main advantage of the chosen primal-dual splitting algorithm is that it allows us to solve (5) for any Lipschitz differentiable function $h$ while allowing arbitrary linear operators $(V_r)_{1\leq r\leq R}$. Another strong point of this algorithm is that it does not require any matrix inversion to be performed at each iteration. Our primal-dual method is summarized in Algorithm 1. It corresponds to an instance of the algorithm proposed recently in [23] under a generic form.

**Algorithm 1** Proposed algorithm.

Let $\gamma \in (0,+\infty)$. Let $(c_k)_{k\in\mathbb{N}}$ and $(e_k)_{k\in\mathbb{N}}$ be some sequences of elements of $\mathbb{R}^N$ corresponding to possible errors in the computation of the gradient of $h$.

**Initialization:**

Set $x_0 \in \mathbb{R}^N$, and $(\forall r \in \{1,\dots,R\})\ v_{r,0} \in \mathbb{R}^{P_r}$.

**Iterations:**

For $k = 0, \dots$

$y_{1,k} = x_k - \gamma\left(\nabla h(x_k) + \sum_{r=1}^R V_r^\top v_{r,k}\right) + c_k$

$p_{1,k} = \mathrm{prox}_{\gamma\psi_0}(y_{1,k})$

For $r = 1, \dots, R$

$y_{2,r,k} = v_{r,k} + \gamma V_r x_k$

$p_{2,r,k} = y_{2,r,k} - \gamma \mathrm{prox}_{\gamma^{-1}\psi_r}(\gamma^{-1} y_{2,r,k})$

$q_{2,r,k} = p_{2,r,k} + \gamma V_r p_{1,k}$

$v_{r,k+1} = v_{r,k} - y_{2,r,k} + q_{2,r,k}$

$q_{1,k} = p_{1,k} - \gamma\left(\nabla h(p_{1,k}) + \sum_{r=1}^R V_r^\top p_{2,r,k}\right) + e_k$

$x_{k+1} = x_k - y_{1,k} + q_{1,k}$

### C. Convergence result

The convergence of the proposed primal-dual proximal splitting algorithm is guaranteed by the following result deduced from Theorem II.1 and [23, Theorem 4.2]:

**Theorem III.2** *Given the following assumptions:*

(i) *$f$ is coercive, i.e. $\lim_{\|x\|\to+\infty} f(x) = +\infty$,*

(ii) *for every $r \in \{1,\dots,R\}$, $\psi_r$ is finite valued,*

(iii) *$\gamma \in [\epsilon, (1-\epsilon)/\delta]$ where $\epsilon \in (0, 1/(\delta+1))$ and*

$$\delta = \mu + \sqrt{\sum_{r=1}^R \|V_r\|^2},$$

(iv) *$(c_k)_{k\in\mathbb{N}}$ and $(e_k)_{k\in\mathbb{N}}$ are absolutely summable sequences,*

*then there exists a minimizer $\widehat{x}$ of (22) such that the sequences $(x_k)_{k\in\mathbb{N}}$ and $(p_{1,k})_{k\in\mathbb{N}}$ converge to $\widehat{x}$.*

### D. Implementation issues

Note that Algorithm 1 is tolerant to numerical errors $(c_k)_{k\in\mathbb{N}}$ and $(e_k)_{k\in\mathbb{N}}$. This feature is essential in our problem, as the gradient of the Poisson-Gaussian negative log-likelihood given by (8) involves infinite sums.

We now propose, for these sums, finite summation bounds that depend on the current estimate of $x$. Let us firstly rewrite

$s(a,b)$ defined in (12) as $s(a,b) = \sum_{n=0}^{+\infty} \Pi(a,b,n)$ with

$$\Pi(a,b,n) = \frac{a^n}{n!} e^{-\left(\frac{b-n}{\sqrt{2}\sigma}\right)^2}. \tag{25}$$

Then, the approximation accuracy is guaranteed by the following result deduced from [51, Proposition A.2]:

**Proposition III.3** *Let $\Delta > 0$ and set*

$$n^- = \lfloor n^* - \Delta\sigma \rfloor, \quad n^+ = \lceil n^* + \Delta\sigma \rceil \tag{26}$$

*with $n^*$ given by*

$$n^* = \sigma^2 \mathsf{W}\left(\frac{a}{\sigma^2} e^{b/\sigma^2}\right), \tag{27}$$

*where $\mathsf{W}(\cdot)$ denotes the Lambert function. Then, $\sum_{n=\max(1,n^-)}^{n^+} \Pi(a,b,n)$ constitutes a lower approximation to $\sum_{n=1}^{+\infty} \Pi(a,b,n)$ with maximum error value*

$$\sqrt{2\pi}\sigma\, \Pi(a,b,n^*) \left(1 - \operatorname{erf}\left(\frac{\Delta}{\sqrt{2}}\right)\right).$$

*where* erf *denotes the error function.*

One can observe in Fig. 1 that the bounds defined in (26) can be quite precise. On the contrary, the summation bounds $n^- = 0$ and $n^+ = b + 4\sigma$ proposed in [11], [52] are not always guaranteed to include all the significant coefficients or to be very effective. Note that efficient numerical methods exist to compute the Lambert function [53].

## IV. Simulations

We now demonstrate the practical performance of our method on image restoration experiments in the context of data corrupted with Poisson-Gaussian noise. More specifically, our study is focused on confocal images. Our simulations aim at illustrating the usefulness of our approach and discuss the merits of the various approximations of the Poisson-Gaussian likelihood. The image resulting from the time series noise identification procedure described in [51] provides ground truth for this experiment. The considered ground truth images, i.e. $\overline{x}_1$ of size $128 \times 128$ and $\overline{x}_2$ of size $190 \times 190$ were acquired using a macro confocal laser scanning microscope (Leica TCS-LSI) and are illustrated in Figs. 2(a) and 3(a), respectively. Additionally we use the publicly available confocal microscopy image $\overline{x}_3$ of size $256 \times 256$ illustrated in Fig. 5(a).[5] First, a study of the influence of the data fidelity choice in terms of image restoration quality is presented. For a data fidelity term $h$ derived from Gaussian likelihood, GAST, EXP, WL2 or given by the exact expression given in (6), the resulting problem involves the minimization of

$$f = h + \iota_C + \sum_{r=1}^{R} \psi_r, \tag{28}$$

where $\iota_C$ is the indicator function of $C = [x^-, x^+]^N$ and $(x^-, x^+) \in [0, +\infty)^2$ defines the expected pixel value range. In the following $x^-$ is set to 0. In the proposed framework, GAST is thus handled in a manner similar to [55], i.e. by taking advantage of Lipschitz-differentiability properties of the function $\widetilde{\Phi}$ in the first line of Table I, as studied in the context of Poisson noise in [55].

[5] www.gensat.org/imagenavigator.jsp?imageID=29109 [54]

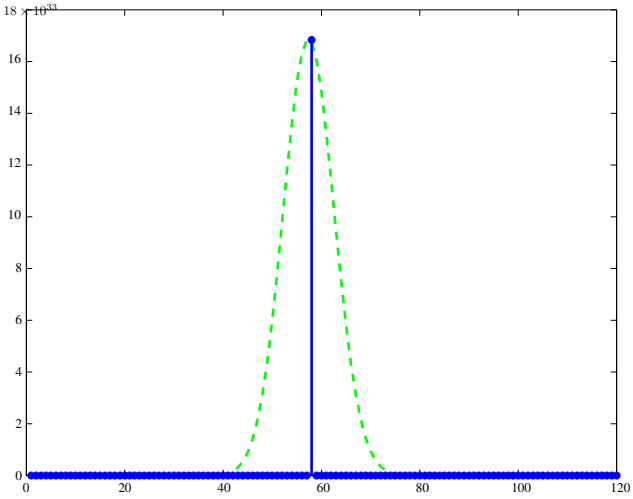


(a) An approximation $n^*$ (marked with a solid blue line) to the maximizer of $\Pi(a,b,n)$ (in dashed green).

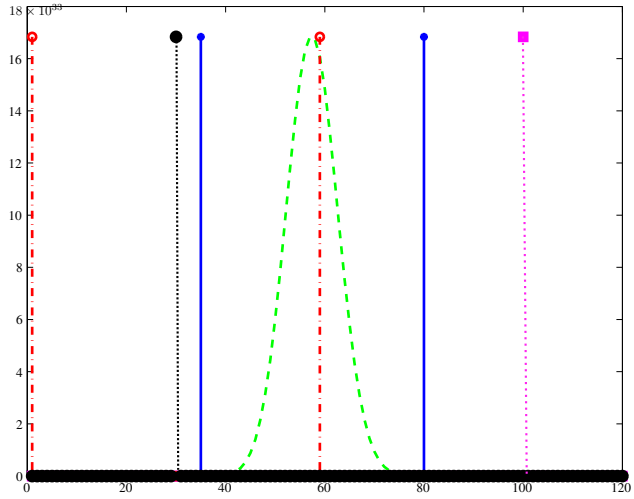


(b) Summation bounds proposed in Proposition III.3 (marked with the solid blue lines) for $\Delta = 3$ and given by $n^- = 0$ and $n^+ = b + 4\sigma$ (marked with the dash-dotted red lines). The dotted lines indicate $a$ (in black with a circle marker) and $b$ (in pink with a square marker), respectively.

Fig. 1. An approximation $n^*$ to the maximizer of function $\Pi(a,b,n)$ (a) and summation bounds proposed in Proposition III.3 (b) for the settings: $a = 100$, $b = 30$ and $\sigma^2 = 50$.

For a data fidelity term corresponding to the exact Poisson likelihood or to SPoiss, we set

$$f = \iota_C + \psi_1 + \sum_{r=2}^{R} \psi_r, \tag{29}$$

where $\psi_1$ denotes a Kullback-Leibler divergence. The observed image is generated by degrading the original image $\overline{x}_1$ with a convolution operator $H$, which corresponds to a truncated Gaussian point spread function of standard deviation 1.6 and kernel size $25 \times 25$. The image is further corrupted with a scaled Poisson noise and a zero-mean additive white Gaussian noise. In this experiment the proposed framework is

| $(x^+, \sigma^2)$ | | Init | Poiss. | Gauss. | GAST [21] | EXP [11] | SPoiss [19] | WL2 [11], [18], [20] | Exact |
|---|---|---|---|---|---|---|---|---|---|
| (15,9) | $\lambda$ | - | 0.146 | 0.140 | 0.069 | 0.081 | 0.077 | 0.079 | 0.080 |
| | MAE | 54.26 | 13.29 | 10.87 | 11.49 | **10.82** | 10.87 | 12.89 | **10.82** |
| | SNR | 6.31 | 18.68 | 19.73 | 19.27 | **19.81** | 19.78 | 18.74 | **19.81** |
| | SSIM | 0.088 | 0.752 | 0.817 | 0.815 | **0.818** | 0.816 | 0.789 | **0.818** |
| (30,12) | $\lambda$ | - | 0.105 | 0.121 | 0.060 | 0.055 | 0.059 | 0.054 | 0.052 |
| | MAE | 34.81 | 9.60 | **8.47** | 8.75 | 8.53 | 8.56 | 9.22 | **8.47** |
| | SNR | 10.72 | 21.14 | 21.60 | 21.39 | 21.61 | 21.61 | 21.25 | **21.72** |
| | SSIM | 0.179 | 0.839 | **0.878** | 0.875 | 0.875 | 0.874 | 0.864 | 0.875 |
| (120,60) | $\lambda$ | - | 0.051 | 0.044 | 0.019 | 0.020 | 0.020 | 0.021 | 0.020 |
| | MAE | 19.64 | 6.79 | **6.19** | 6.22 | 6.22 | 6.21 | 6.28 | 6.21 |
| | SNR | 14.85 | 23.85 | 24.22 | 24.30 | **24.31** | **24.31** | 24.27 | **24.31** |
| | SSIM | 0.367 | 0.904 | **0.927** | 0.926 | 0.925 | 0.926 | 0.924 | 0.925 |

TABLE II
INTENSITY LEVEL INFLUENCE ON RESTORING IMAGE $\overline{x}_1$ DEGRADED WITH A CONVOLUTION OPERATOR $H$ CORRESPONDING TO A TRUNCATED GAUSSIAN POINT SPREAD FUNCTION OF STANDARD DEVIATION 1.6 WITH KERNEL SIZE $25 \times 25$ AND CORRUPTED WITH POISSON-GAUSSIAN NOISE.

applied to Non Local Total Variation (NLTV) restoration. The linear operators $V_r$ associated with NLTV are computed from an initial Wiener filter restoration using code by Bresson [56].[6] The NLTV prior term is weighted by a regularization constant $\lambda > 0$. In all our experiments, this parameter is tuned so as to minimize the Mean Absolute Error (MAE) between the original image $\bar{x}$ and its estimate $\hat{x}$. The quality of the results is evaluated in terms of MAE, SNR and SSIM [57]. The provided relative MAE values are normalized with a factor $255/x^+$. One can observe by inspecting the evaluation scores in Table II, that the exact model overall leads to the best quantitative results. In the case of Poisson, SPoiss, WL2 and GAST data fidelity terms, the required convexity conditions (see Table I) of the observation image is ensured by data truncation. The associated results provided in Table II show that the Poisson, WL2 and GAST strategies lead to relatively lower performance.

Next a study of penalization strategies for low-count image is presented. As mentioned previously, the problem formulation given in (22) allows us to address a wide range of problems. For the sake of illustration we consider the restoration with three penalization strategies, namely TV, NLTV and hybrid regularization, which integrates TV and a Hessian prior [37]. TV and Hessian designate the total variation and second-order difference-based semi-norms defined in Section III-A, respectively. We use three images: the same images as previously $\overline{x}_1$ with $x^+ = 30$, $\overline{x}_2$ with $x^+ = 12$ and $\overline{x}_3$ with $x^+ = 60$. The original images $\overline{x}_1$ and $\overline{x}_2$ are degraded with the same convolutive operator $H$ as previously, further corrupted with a Poisson noise and a zero-mean additive white Gaussian noise with noise variance $\sigma^2 = 12$ and $\sigma^2 = 9$, respectively. The original image $\overline{x}_3$ was degraded with a convolution operator $H$ corresponding to a truncated Gaussian point spread function with standard deviation $0.5$ and kernel size $9 \times 9$, corrupted with a Poisson noise and a zero-mean additive Gaussian noise with noise variance $\sigma^2 = 36$. All the provided examples illustrate the performance of the proposed technique for image restoration with fairly low initial SNR, i.e. only $10.05$ dB, $2.19$ dB and $9.37$ dB for the images given in Figs. 2(b), 4(b) and 5(b), respectively. By inspecting the numerical evaluation scores presented in Tables III, IV and V one can conclude that the performance gain obtained by using the exact data fidelity term is independent of the chosen regularization strategy.

The Gaussian and EXP data fidelity terms may be very competitive as illustrated in Table IV. However in some instances the performance gain between the exact and Gaussian data fidelity term is significant (see Table III). One can observe in Figs. 2(e) and 5(e) that the hybrid Hessian-TV regularization strategy leads to very good results. This can be also validated by inspecting the final MAE relative value equal to $7.90$, $7.53$ and $11.29$, the SNR improvement (ISNR) equal to $11.54$ dB, $17.61$ dB and $6.45$ dB for the first, the second and the third image, respectively. The NLTV regularization strategy does not perform as well for the experiment presented in Table IV. This reflects the fact that the similarity between local image features is essentially lost in the initial image (Fig. 3(b), SNR = $2.19$ dB). Consequently, the NLTV weights cannot be adjusted properly.

Finally, in Table VI, we illustrate the influence of the choice of parameter $\Delta$. One can observe that the restoration performance is stable for $\Delta \geq 3$.

Complementary to these numerical results, Figs. 2, 4 and 5 illustrate the visual differences resulting from various data fidelity terms and regularization strategies. One can observe that a higher number of low intensity components are lost when using a data fidelity term derived from Poisson statistics (Fig. 4(a)). The shape of low intensity component is also not well reconstructed when using a WL2 data fidelity term (Fig. 4(f)). Most artifacts are corrected when using the GAST data fidelity term (Fig. 4(c)) while even better results are obtained with the Gaussian and SPoiss (Figs. 4(b)-(e)). Finally, one can hardly find a visual difference between the EXP approximation (Fig. 4(d)) and the exact data fidelity term (Fig. 3(c)). The NLTV regularization term should have reduced

[6] http://www.cs.cityu.edu.hk/∼xbresson/codes.html

| | | Poiss. | Gauss. | GAST [21] | EXP [11] | SPoiss [19] | WL2 [11], [18], [20] | Exact |
|---|---|---|---|---|---|---|---|---|
| TV | $\lambda$ | 0.164 | 0.197 | 0.093 | 0.096 | 0.095 | 0.099 | 0.093 |
| | MAE | 10.71 | 9.42 | 9.73 | 9.49 | 9.50 | 10.05 | **9.14** |
| | SNR | 20.21 | 20.79 | 20.55 | 20.79 | 20.79 | 20.57 | **21.15** |
| | SSIM | 0.814 | 0.859 | 0.858 | 0.858 | 0.858 | 0.846 | **0.864** |
| NLTV | $\lambda$ | 0.105 | 0.121 | 0.060 | 0.055 | 0.059 | 0.054 | 0.052 |
| | MAE | 9.60 | **8.47** | 8.75 | 8.53 | 8.56 | 9.22 | **8.47** |
| | SNR | 21.14 | 21.60 | 21.39 | 21.61 | 21.61 | 21.25 | **21.72** |
| | SSIM | 0.839 | **0.878** | 0.875 | 0.875 | 0.874 | 0.864 | 0.875 |
| TV + Hessian | $\lambda_{\text{TV}}$ | 0.043 | 0.075 | 0.027 | 0.031 | 0.030 | 0.037 | 0.031 |
| | $\lambda_{\text{H}}$ | 0.148 | 0.136 | 0.070 | 0.072 | 0.070 | 0.059 | 0.070 |
| | MAE | 8.99 | 7.93 | 8.18 | 7.92 | 7.93 | 8.70 | **7.90** |
| | SNR | 21.09 | 21.54 | 21.30 | 21.59 | 21.60 | 21.25 | **21.61** |
| | SSIM | 0.861 | 0.899 | 0.899 | 0.899 | 0.899 | 0.887 | **0.900** |

TABLE III
PENALIZATION STRATEGIES FOR LOW-COUNT IMAGE $\overline{x}_1$ ($x^+ = 30$) DEGRADED WITH A CONVOLUTION OPERATOR $H$ CORRESPONDING TO A TRUNCATED GAUSSIAN POINT SPREAD FUNCTION OF STANDARD DEVIATION 1.6 WITH KERNEL SIZE $25 \times 25$ AND CORRUPTED WITH POISSON-GAUSSIAN NOISE, NOISE VARIANCE $\sigma^2 = 12$ (MAE = 34.81, SNR = 10.07 DB, SSIM = 0.178).

| | | Poiss. | Gauss. | GAST [21] | EXP [11] | SPoiss [19] | WL2 [11], [18], [20] | Exact |
|---|---|---|---|---|---|---|---|---|
| TV | $\lambda$ | 0.338 | 0.218 | 0.155 | 0.156 | 0.153 | 0.133 | 0.154 |
| | MAE | 11.70 | 8.79 | 9.76 | 8.68 | 8.78 | 12.90 | **8.66** |
| | SNR | 16.73 | 18.74 | 17.73 | 18.80 | 18.72 | 16.18 | **18.81** |
| | SSIM | 0.758 | 0.788 | 0.783 | **0.790** | 0.787 | 0.770 | **0.790** |
| NLTV | $\lambda$ | 0.243 | 0.164 | 0.115 | 0.114 | 0.117 | 0.101 | 0.138 |
| | MAE | 12.03 | **9.25** | 10.15 | 9.26 | 9.31 | 13.20 | **9.25** |
| | SNR | 16.57 | **18.38** | 17.50 | 18.36 | 18.33 | 15.92 | **18.38** |
| | SSIM | 0.733 | **0.759** | 0.755 | 0.757 | 0.757 | 0.739 | 0.758 |
| TV + Hessian | $\lambda_{\text{TV}}$ | 0.016 | 0.004 | 0.016 | 0.012 | 0.013 | 0.051 | 0.008 |
| | $\lambda_{\text{H}}$ | 0.609 | 0.472 | 0.293 | 0.297 | 0.292 | 0.119 | 0.296 |
| | MAE | 10.89 | 7.62 | 8.70 | **7.53** | 7.63 | 12.46 | **7.53** |
| | SNR | 17.30 | 19.72 | 18.60 | **19.81** | 19.72 | 16.58 | **19.81** |
| | SSIM | 0.815 | 0.845 | 0.839 | **0.846** | 0.844 | 0.812 | **0.846** |

TABLE IV
PENALIZATION STRATEGIES FOR LOW-COUNT IMAGE $\overline{x}_2$ ($x^+ = 12$) DEGRADED WITH A CONVOLUTION OPERATOR $H$ CORRESPONDING TO A TRUNCATED GAUSSIAN POINT SPREAD FUNCTION OF STANDARD DEVIATION 1.6 WITH KERNEL SIZE $25 \times 25$ AND CORRUPTED WITH POISSON-GAUSSIAN NOISE, NOISE VARIANCE $\sigma^2 = 9$ (MAE = 61, SNR = 2.19 DB, SSIM = 0.022).

the undesired staircase effect visible in the TV result (see Fig. 2(c)) but for the considered low SNR observed images the improvement is actually only incremental (see Fig. 2(d)). In contrast, the Hessian-TV regularization appears to be more effective in alleviating this effect (see Fig. 2(e)).

## V. CONCLUSION

We have shown that Poisson-Gaussian neg-log-likelihood is a convex, Lipschitz-differentiable function. The provided convexity result is actually more general as it applies to the neg-log likelihood of a mixture of Generalized-Gaussian and Poisson variables. Building upon these results, we have proposed a new variational approach for solving data recovery problems in the presence of Poisson-Gaussian noise. We have developed a practical implementation of an efficient primal-dual algorithm, which is particularly flexible, i.e. for which a large range of penalization strategies and data fidelity terms are applicable. Among those we employed, the hybrid TV-Hessian prior was shown to produce naturally looking, high quality results for low count microscopy image restoration problems in the presence of Poisson-Gaussian noise. We have shown the good performance of our restoration algorithm using the exact data fidelity term and various approximations. In addition, we also conclude that the EXP and SPoiss fidelity terms provide good results compared to the exact solution. In a future work we would like to extend our approach to encompass the case of Generalized Gaussian-Poisson noise and to study the performance of other regularization strategies than those we have considered here. Although only TV, NLTV and hybrid TV-Hessian priors were analyzed in this work, the versatility of our approach should allow us to address a variety

| | | Poiss. | Gauss. | GAST [21] | EXP [11] | SPoiss [19] | WL2 [11], [18], [20] | Exact |
|---|---|---|---|---|---|---|---|---|
| TV | $\lambda$ | 0.299 | 0.116 | 0.078 | 0.078 | 0.078 | 0.075 | 0.077 |
| | MAE | 13.55 | 11.89 | 11.79 | **11.69** | 11.73 | 11.80 | **11.69** |
| | SNR | 14.41 | 15.42 | 15.39 | 15.48 | 15.46 | **15.49** | **15.49** |
| | SSIM | 0.724 | 0.759 | 0.762 | 0.766 | 0.764 | **0.767** | 0.766 |
| NLTV | $\lambda$ | 0.301 | 0.118 | 0.078 | 0.077 | 0.077 | 0.074 | 0.076 |
| | MAE | 12.28 | 12.21 | 11.79 | 11.77 | 11.78 | 11.91 | **11.75** |
| | SNR | 15.10 | 15.16 | 15.40 | 15.44 | **15.45** | 15.43 | **15.45** |
| | SSIM | 0.742 | 0.742 | 0.759 | 0.759 | 0.758 | **0.760** | 0.759 |
| TV + Hessian | $\lambda_{\text{TV}}$ | 0.050 | 0.037 | 0.052 | 0.030 | 0.046 | 0.046 | 0.027 |
| | $\lambda_{\text{H}}$ | 0.127 | 0.054 | 0.052 | 0.034 | 0.027 | 0.020 | 0.030 |
| | MAE | 11.97 | 11.33 | 11.44 | **11.29** | 11.30 | 11.45 | **11.29** |
| | SNR | 15.24 | 15.76 | 15.64 | 15.77 | 15.79 | 15.73 | **15.82** |
| | SSIM | 0.760 | 0.775 | 0.768 | **0.782** | 0.778 | 0.779 | 0.781 |

TABLE V
PENALIZATION STRATEGIES FOR LOW-COUNT IMAGE $\overline{x}_3$ ($x^+ = 60$) DEGRADED WITH A CONVOLUTION OPERATOR $H$ CORRESPONDING TO A TRUNCATED GAUSSIAN POINT SPREAD FUNCTION OF STANDARD DEVIATION 0.5 WITH KERNEL SIZE $9 \times 9$ AND CORRUPTED WITH POISSON-GAUSSIAN NOISE, NOISE VARIANCE $\sigma^2 = 36$ (MAE = 25.17, SNR = 9.37 DB, SSIM = 0.506).

| $\Delta$ | 0.33 | 0.5 | 1 | 2 | 3 | 4 | 5 |
|---|---|---|---|---|---|---|---|
| MAE | 8.10 | 7.98 | 7.89 | 7.90 | 7.90 | 7.90 | 7.90 |
| SNR | 21.51 | 21.57 | 21.63 | 21.61 | 21.61 | 21.61 | 21.61 |
| SSIM | 0.892 | 0.897 | 0.898 | 0.899 | 0.900 | 0.900 | 0.900 |

Image $\overline{x}_1$, ($x^+ = 30$) degraded with $H$ corresponding to a truncated Gaussian PSF of standard deviation 1.6 with kernel size $25 \times 25$ , $\sigma^2 = 12$ (MAE = 35, SNR = 10.07 dB, SSIM = 0.178)

| $\Delta$ | 0.33 | 0.5 | 1 | 2 | 3 | 4 | 5 |
|---|---|---|---|---|---|---|---|
| MAE | 10.98 | 9.30 | 7.69 | 7.53 | 7.53 | 7.53 | 7.53 |
| SNR | 17.42 | 18.51 | 19.72 | 19.81 | 19.81 | 19.81 | 19.81 |
| SSIM | 0.832 | 0.841 | 0.846 | 0.846 | 0.846 | 0.846 | 0.846 |

Image $\overline{x}_2$, ($x^+ = 12$) degraded with $H$ corresponding to a truncated Gaussian PSF of standard deviation 1.6 with kernel size $25 \times 25$, $\sigma^2 = 9$ (MAE = 61, SNR = 2.19 dB, SSIM = 0.022)

| $\Delta$ | 0.33 | 0.5 | 1 | 2 | 3 | 4 | 5 |
|---|---|---|---|---|---|---|---|
| MAE | 11.36 | 11.34 | 11.30 | 11.29 | 11.29 | 11.29 | 11.29 |
| SNR | 15.81 | 15.81 | 15.83 | 15.82 | 15.82 | 15.82 | 15.82 |
| SSIM | 0.783 | 0.783 | 0.784 | 0.784 | 0.783 | 0.783 | 0.783 |

Image $\overline{x}_3$, ($x^+ = 60$) degraded with $H$ corresponding to a truncated Gaussian PSF of standard deviation 0.5 with kernel size $9 \times 9$, $\sigma^2 = 36$ (MAE = 25.17, SNR = 9.37 dB, SSIM = 0.506)

TABLE VI
INFLUENCE OF $\Delta$ ON RESTORATION RESULTS. IMAGES RECONSTRUCTED WITH HESSIAN-TV PRIOR.

of applications by making use of various forms of convex penalty functions.

## APPENDIX A
## PROOF OF THEOREM II.1

Our proof consists of showing that, for every $i \in \{1, \cdots, Q\}$, $\eta_i$ is upper bounded on $[0, +\infty)$ by $\eta_i(0)$, where $\eta_i(0)$ is defined in (21). Firstly, we recall that for $a = 0$ the infinite sum (12) simplifies to the first sum element. Consequently, for every $z_i \in (0, +\infty)$, we have the following equivalences:

$$
\begin{aligned}
&\eta_i(0) - \eta_i(z_i) \geq 0 \qquad (30)\\
&\Leftrightarrow (s(z_i, y_i))^2 \eta_i(0) - \\
&\qquad \Big((s(z_i, y_i - 1))^2 - s(z_i, y_i)s(z_i, y_i - 2)\Big) \geq 0\\
&\Leftrightarrow \sum_{m=0}^{\infty}\sum_{n=0}^{\infty} \frac{z_i^{m+n}}{m!n!} \left( e^{\frac{-(y_i-m)^2-(y_i-n)^2}{2\sigma^2}} \eta_i(0) - \right.\\
&\qquad \left. e^{\frac{-(y_i-1-m)^2-(y_i-1-n)^2}{2\sigma^2}} + e^{\frac{-(y_i-m)^2-(y_i-2-n)^2}{2\sigma^2}} \right) \geq 0\\
&\Leftrightarrow \sum_{m=0}^{\infty}\sum_{n=0}^{\infty} \frac{z_i^{m+n}}{m!n!} e^{\frac{-(y_i-n)^2-(y_i-m)^2+4y_i-2}{2\sigma^2}}\\
&\qquad \times \left\{1 - e^{-\frac{n+m}{\sigma^2}} + e^{-\frac{1}{\sigma^2}} \left(e^{-\frac{2n}{\sigma^2}} - 1\right)\right\} \geq 0\\
&\Leftrightarrow \sum_{m=0}^{\infty}\sum_{n=0}^{m-1} \frac{z_i^{m+n}}{m!n!} e^{\frac{-(y_i-n)^2-(y_i-m)^2+4y_i-2}{2\sigma^2}}\\
&\times \left\{2\left(1 - e^{-\frac{n+m}{\sigma^2}}\right)\left(1 - e^{-\frac{1}{\sigma^2}}\right) + e^{-\frac{1}{\sigma^2}} \left(e^{-\frac{n}{\sigma^2}} - e^{-\frac{m}{\sigma^2}}\right)^2\right\}\\
&+ \sum_{m=0}^{\infty} \frac{z_i^{2m}}{(m!)^2} e^{\frac{-(y_i-m)^2+2y_i-1}{\sigma^2}} (1 - e^{-\frac{2m}{\sigma^2}})(1 - e^{-\frac{1}{\sigma^2}}) \geq 0.
\end{aligned}
$$

The latter inequality holds, since the left-hand side is a sum of nonnegative terms. Hence, the expression of the Lipschitz constant $\mu$ in (13) is obtained by searching the maximum value of $\eta_i(0)$ for all possible values of $i \in \{1, \ldots, Q\}$.

## APPENDIX B
## PROOF OF THEOREM II.2

It is sufficient to show that, for every $i \in \{1, \cdots, Q\}$,

$$
(\forall a \in (0, +\infty)) \quad \begin{cases} \ddot{\Phi}_i^{(\beta)}(a) > 0 \ \text{ if } \beta > 1, \\ \ddot{\Phi}_i^{(\beta)}(a) \geq 0 \ \text{ if } \beta = 1, \end{cases} \qquad (31)
$$

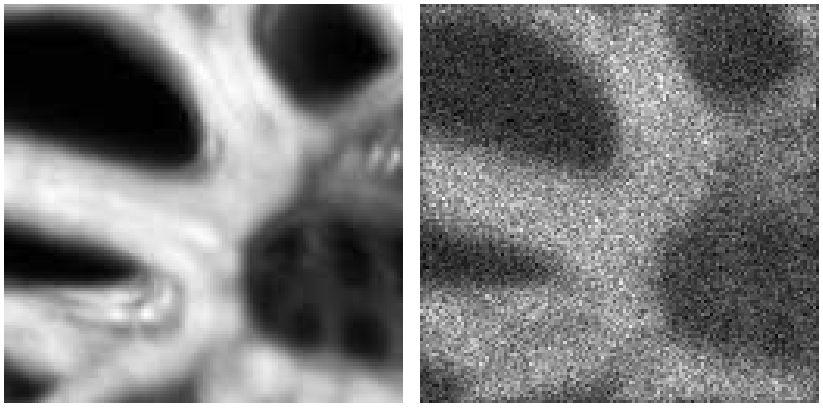

(a) Original $\overline{x}_1$ ($x^+ = 30$) (b) Degraded (MAE = 35, SNR = 10.07 dB)

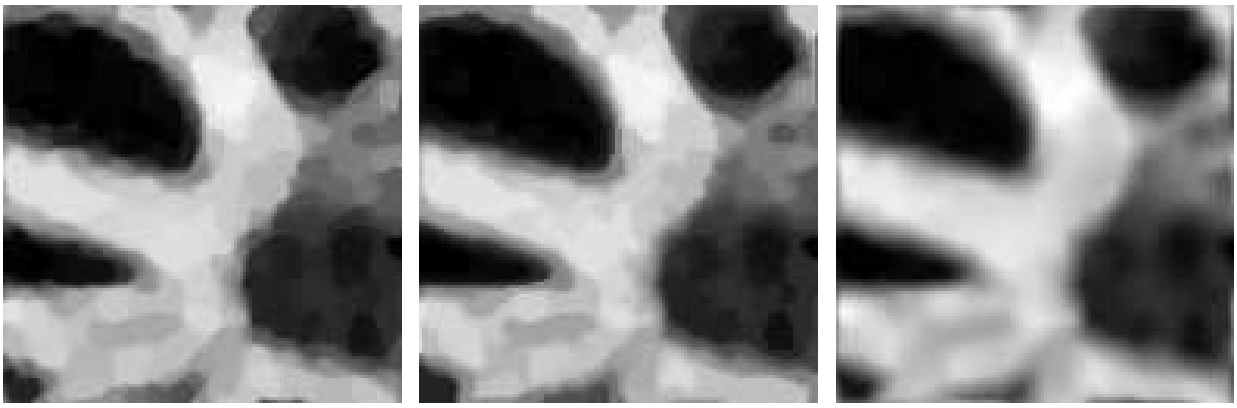

(c) Restoration result with TV prior (MAE = 9.14 , SNR = 21.15 dB, ISNR = 11.08 dB, SSIM = 0.864) (d) Restoration result with NLTV prior (MAE = 8.47 , SNR = 21.72 dB, ISNR = 11.65 dB, SSIM = 0.875) (e) Restoration result with Hessian-TV prior (MAE = 7.91 , SNR = 21.52 dB, ISNR = 11.44 dB, SSIM = 0.854)

Fig. 2. An example of macroconfocal image restored with our proposed techniques. (A) was degraded by a $25 \times 25$ truncated Gaussian blur with standard deviation 1.6 and corrupted with Poisson-Gaussian noise ($\sigma^2 = 12$). Image results obtained with exact data fidelity term and various prior terms.

where

$$\ddot{\Phi}_i^{(\beta)}(a) = \left(\left(s^{(\beta)}(a, y_i - 1)\right)^2 - s^{(\beta)}(a, y_i)s^{(\beta)}(a, y_i - 2)\right) / \left(s^{(\beta)}(a, y_i)\right)^2, \tag{32}$$

and, for every $b \in \mathbb{R}$,

$$s^{(\beta)}(a, b) = \sum_{n=0}^{+\infty} \frac{a^n}{n!} \zeta_b^{(\beta)}(n), \tag{33}$$

with $\zeta_b^{(\beta)}(\cdot) = e^{-\left(\frac{|\cdot - b|}{\sqrt{2}\sigma}\right)^\beta}$. The proof reduces to studying the sign of the numerator of $\ddot{\Phi}_i^{(\beta)}$. For every $a \in [0, +\infty)$, $b \in \mathbb{R}$ and $\beta \in (0, +\infty)$, the following equivalences hold:

$$\begin{aligned}
&\left(s^{(\beta)}(a, b-1)\right)^2 - s^{(\beta)}(a, b)s^{(\beta)}(a, b-2) \geq 0 \qquad (34)\\
&\Leftrightarrow \sum_{m=0}^{\infty}\sum_{n=0}^{\infty} \frac{a^{n+m}}{n!m!} \\
&\quad \left(\zeta_b^{(\beta)}(m+1)\zeta_b^{(\beta)}(n+1) - \zeta_b^{(\beta)}(m)\zeta_b^{(\beta)}(n+2)\right) \geq 0 \\
&\Leftrightarrow \sum_{m=0}^{\infty}\sum_{n=0}^{\infty} \frac{a^{n+m-1}}{n!m!} n \\
&\quad \times \left(\zeta_b^{(\beta)}(m+1)\zeta_b^{(\beta)}(n) - \zeta_b^{(\beta)}(m)\zeta_b^{(\beta)}(n+1)\right) \geq 0 \\
&\Leftrightarrow \sum_{m=0}^{\infty}\left\{\sum_{n=0}^{m} \frac{a^{n+m-1}}{n!m!} n \left(\zeta_b^{(\beta)}(m+1)\zeta_b^{(\beta)}(n) - \right.\right. \\
&\quad \left.\zeta_b^{(\beta)}(m)\zeta_b^{(\beta)}(n+1)\right) + \sum_{n=m}^{\infty} \frac{a^{n+m-1}}{n!m!} n \\
&\quad \left.\times \left(\zeta_b^{(\beta)}(m+1)\zeta_b^{(\beta)}(n) - \zeta_b^{(\beta)}(m)\zeta_b^{(\beta)}(n+1)\right)\right\} \geq 0 \\
&\Leftrightarrow \sum_{m=0}^{\infty}\left\{\sum_{n=0}^{m} \frac{a^{n+m-1}}{n!m!} n \left(\zeta_b^{(\beta)}(m+1)\zeta_b^{(\beta)}(n) - \right.\right. \\
&\quad \left.\zeta_b^{(\beta)}(m)\zeta_b^{(\beta)}(n+1)\right) + \sum_{n=0}^{m} \frac{a^{n+m-1}}{n!m!} m \\
&\quad \left.\times \left(\zeta_b^{(\beta)}(n+1)\zeta_b^{(\beta)}(m) - \zeta_b^{(\beta)}(n)\zeta_b^{(\beta)}(m+1)\right)\right\} \geq 0 \\
&\Leftrightarrow \sum_{m=0}^{\infty}\sum_{n=0}^{m} \frac{a^{n+m-1}}{n!m!} (m-n) \\
&\quad \times \left(\zeta_b^{(\beta)}(n+1)\zeta_b^{(\beta)}(m) - \zeta_b^{(\beta)}(n)\zeta_b^{(\beta)}(m+1)\right) \geq 0.
\end{aligned}$$

Furthermore, for all $a \in (0, +\infty)$, $b \in \mathbb{R}$, and $(n, m) \in \mathbb{N}^2$

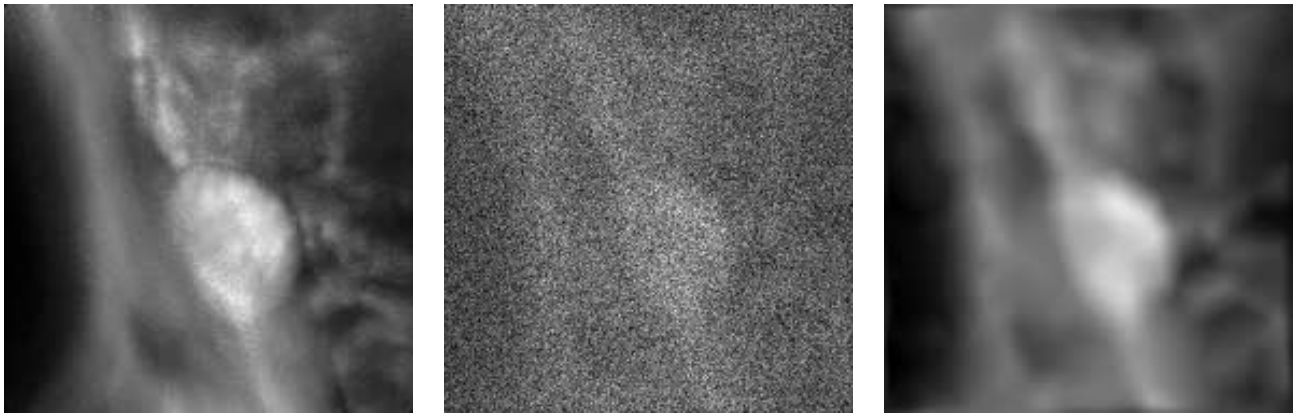

a) Original $\overline{x}_2$ ($x^+ = 12$) b) Degraded (MAE=61, SNR=2.19 dB) c) Exact (MAE=7.53, SNR=19.81 dB)

Fig. 3. The original $\overline{x}_2$, its degraded version and reconstructed with exact Poisson-Gaussian data fidelity term and a Hessian-TV prior.

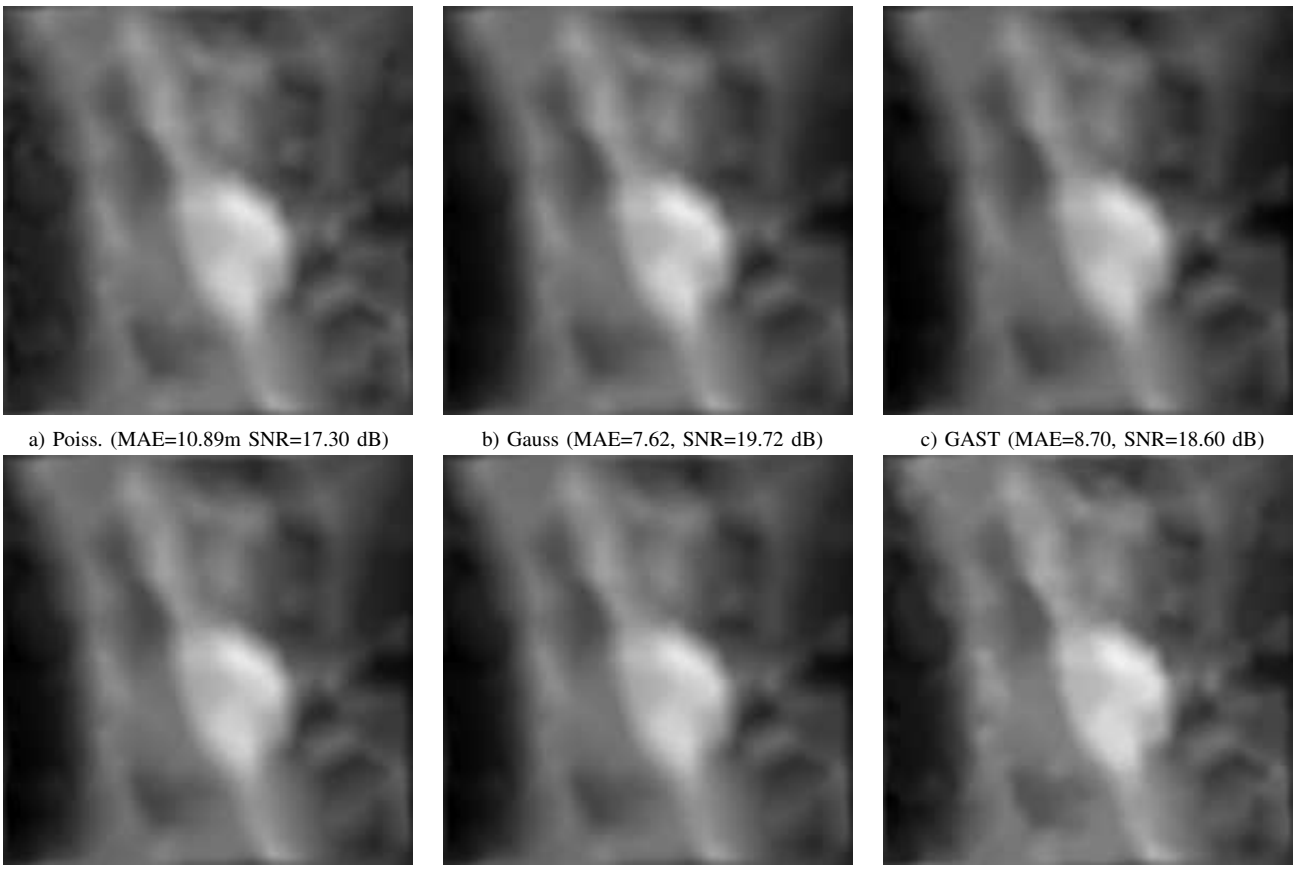

a) Poiss. (MAE=10.89m SNR=17.30 dB) b) Gauss (MAE=7.62, SNR=19.72 dB) c) GAST (MAE=8.70, SNR=18.60 dB)

d) EXP (MAE=7.53, SNR=19.81 dB) e) SPoiss (MAE=7.63, SNR=19.72 dB) f) WL2 (MAE = 12.46, SNR=16.58 dB)

Fig. 4. The image $\overline{x}_2$ reconstructed with various approximation of the Poisson-Gaussian neg-log likelihood and a Hessian-TV prior.

with $m > n$,

$$
\begin{aligned}
&\frac{a^{n+m-1}}{n!m!}(m-n) \\
&\left(\zeta_b^{(\beta)}(n+1)\zeta_b^{(\beta)}(m) - \zeta_b^{(\beta)}(n)\zeta_b^{(\beta)}(m+1)\right) \geq 0 \\
&\Leftrightarrow \zeta_b^{(\beta)}(n+1)\zeta_b^{(\beta)}(m) - \zeta_b^{(\beta)}(n)\zeta_b^{(\beta)}(m+1) \geq 0 \\
&\Leftrightarrow \exp\left(-\left(\frac{|b-n-1|}{\sigma}\right)^{\beta} - \left(\frac{|b-m|}{\sigma}\right)^{\beta}\right) \\
&\qquad - \exp\left(-\left(\frac{|b-n|}{\sigma}\right)^{\beta} - \left(\frac{|b-m-1|}{\sigma}\right)^{\beta}\right) \geq 0 \\
&\Leftrightarrow |b-n|^{\beta} - |b-n-1|^{\beta} \\
&\qquad - \left(|b-m|^{\beta} - |b-m-1|^{\beta}\right) \geq 0. \qquad (35)
\end{aligned}
$$

The above inequality holds if the function

$$
\begin{aligned}
\pi^{(\beta)} \; &: \mathbb{R} \to \mathbb{R} \\
&u \mapsto |u|^{\beta} - |u-1|^{\beta} \qquad (36)
\end{aligned}
$$

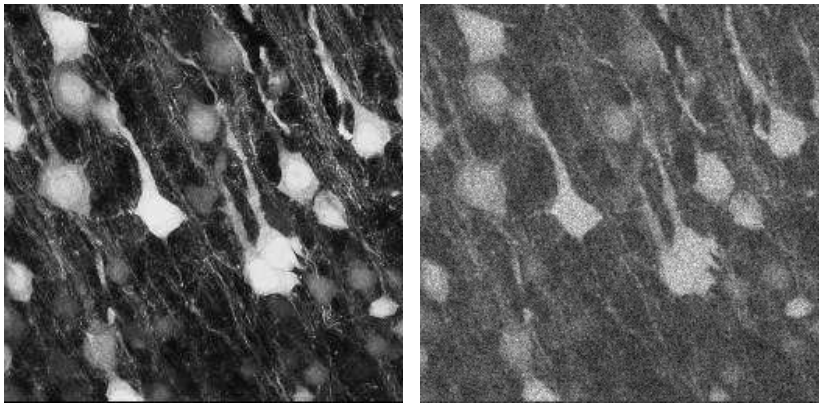

(a) Original $\overline{x}_3$ ($x^+ = 60$) (b) Degraded (MAE = 25.27, SNR = 9.37 dB)

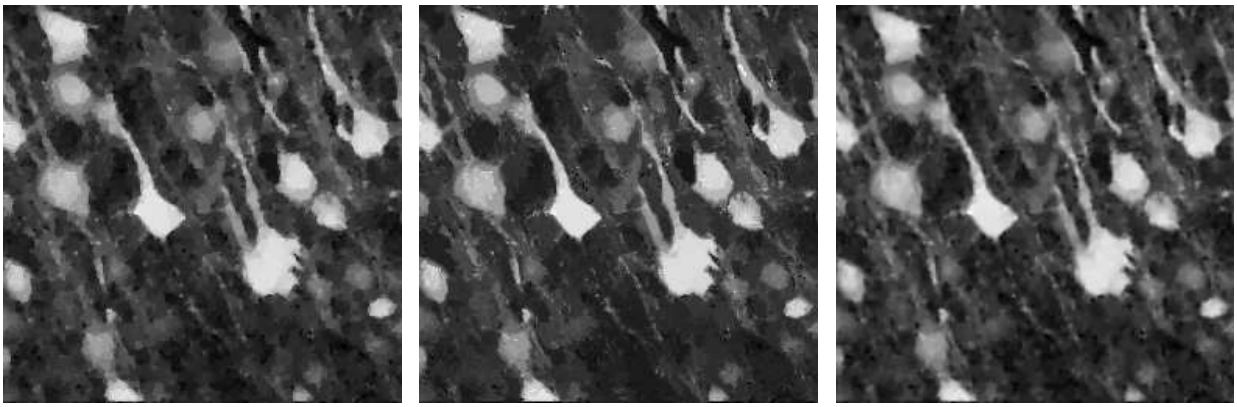

(c) Restoration result obtained with TV prior (MAE = 11.69 , SNR = 15.49 dB, ISNR = 6.12 dB, SSIM = 0.766)

(d) Restoration result obtained with NLTV prior (MAE = 11.75 , SNR = 15.45 dB, ISNR = 6.08 dB, SSIM = 0.759)

(e) Restoration result obtained with Hessian-TV prior (MAE = 11.29 , SNR = 15.82 dB, ISNR = 6.45 dB, SSIM = 0.781)

Fig. 5. An example of confocal image restored with our proposed techniques. The original image (a) was degraded by a $9 \times 9$ truncated Gaussian blur with standard deviation 0.5 and Poisson-Gaussian noise ($\sigma^2 = 36$). Image results were obtained with exact data fidelity term and various prior terms.

is increasing. To prove this fact, let us study the sign of the derivative of the function $\pi^{(\beta)}$ over its domain. The singularity points, i.e. $u \in \{0, 1\}$, can be excluded from the study due to the continuity of $\pi^{(\beta)}$. Then, for $\beta \geq 1$ and $u \in \mathbb{R} \setminus \{0, 1\}$ the derivative is given by

$$\frac{\partial \pi^{(\beta)}(u)}{\partial u} = \beta \left(\text{sign}(u)\,|u|^{\beta-1} - \text{sign}(u-1)\,|u-1|^{\beta-1}\right) = \begin{cases} \beta \left(|u|^{\beta-1} + |u-1|^{\beta-1}\right) & \text{if } u \in (0,1)\,, \\ \beta\, \text{sign}(u)(|u|^{\beta-1} - |u-1|^{\beta-1}) & \text{if } u \in (-\infty, 0) \cup (1, \infty), \end{cases} \tag{37}$$

where sign denotes the signum function, and

$$\text{sign}\left(\frac{\partial \pi^{(\beta)}(u)}{\partial u}\right) = \begin{cases} \text{sign}\left(1 - |u/(u-1)|^{\beta-1}\right) & \text{if } u \in (-\infty, 0)\,, \\ \text{sign}\left(|u/(u-1)|^{\beta-1} + 1\right) & \text{if } u \in (0,1)\,, \\ \text{sign}\left(|u/(u-1)|^{\beta-1} - 1\right) & \text{if } u \in (1, +\infty)\,. \end{cases} \tag{38}$$

Hence, it is positive (resp. nonnegative) for $\beta > 1$ (resp. $\beta = 1$), so that $\pi^{(\beta)}$ is strictly increasing (resp. increasing).

## REFERENCES


[1] A. Jezierska, E. Chouzenoux, J.-C. Pesquet, and H. Talbot, "A primal-dual proximal splitting approach for restoring data corrupted with Poisson-Gaussian noise," in *Proc. Int. Conf. Acoust., Speech Signal Process. (ICASSP 2012)*, Kyoto, Japan, 25-30 Mar. 2012.

[2] C. Chaux, J.-C. Pesquet, and N. Pustelnik, "Nested iterative algorithms for convex constrained image recovery problem," *SIAM J. Imag. Sci.*, vol. 2, no. 2, pp. 730–762, Jun. 2009.

[3] S. Harizanov, J.-C. Pesquet, and G. Steidl, *Epigraphical Projection for Solving Least Squares Anscombe Transformed Constrained Optimization Problems*, vol. 7893 of *Lecture Notes in Computer Science*, pp. 125–136, 2013.

[4] S. Anthoine, J.-F. Aujol, Y. Boursier, and C. Melot, "Some proximal methods for CBCT and PET tomography," *Proc. SPIE*, vol. 8138, pp. 81381E–81381E–12, 2011.

[5] F.-X. Dupé, J. M. Fadili, and J.-L. Starck, "Deconvolution under Poisson noise using exact data fidelity and synthesis or analysis sparsity priors," *Statistiscal Methodology*, vol. 9, no. 1-2, pp. 4–18, 2012.

[6] T. Jeong, H. Woo, and S. Yun, "Frame-based Poisson image restoration using a proximal linearized alternating direction method," *Inverse Probl.*, vol. 29, no. 7, pp. 075007, 2013.

[7] J.-F. Cai, R. H. Chan, and M. Nikolova, "Fast two-phase image deblurring under impulse noise," *J. Math. Imaging Vis.*, vol. 36, no. 1, pp. 46–53, 2010.

[8] G. Aubert and J.-F. Aujol, "A variational approach to removing multiplicative noise," *SIAM J. Appl. Math.*, vol. 68, no. 4, pp. 925–946, 2008.

[9] Y. Xiao, T. Zeng, J. Yu, and M. K. Ng, "Restoration of images corrupted by mixed Gaussian-impulse noise via $\ell_1$-$\ell_0$ minimization," *Pattern Recogn.*, vol. 44, no. 8, pp. 1708 – 1720, 2011.

[10] M. Yan, "Restoration of images corrupted by impulse noise and mixed Gaussian impulse noise using blind inpainting," Tech. Rep., Apr. 2013, http://arxiv.org/abs/1304.1408.

[11] F. Benvenuto, A. La Camera, C. Theys, A. Ferrari, H. Lantéri, and M. Bertero, "The study of an iterative method for the reconstruction of images corrupted by Poisson and Gaussian noise," *Inverse Probl.*, vol. 24, no. 3, 2008, 20 pp.

[12] D. L. Snyder, A. M. Hammoud, and R. L. White, "Image recovery from data acquired with a charge-coupled-device camera," *J. Opt. Soc. Am. A*, vol. 10, no. 5, pp. 1014–1023, May 1993.

[13] T. E. Nichols, J. Qi, E. Asma, and R. M. Leahy, "Spatiotemporal reconstruction of list-mode PET data," *IEEE T. Med. Imaging*, vol. 21, no. 4, pp. 396–404, Apr. 2002.

[14] S. Delpretti, F. Luisier, S. Ramani, T. Blu, and M. Unser, "Multiframe sure-let denoising of timelapse fluorescence microscopy images," in *Proc. IEEE Int. Symp. Biomedical Imaging (ISBI 2008)*, Paris, France, 14-17 May 2008, pp. 149–152.

[15] F. Luisier, T. Blu, and M. Unser, "Image denoising in mixed Poisson-Gaussian noise," *IEEE Trans. Image Process.*, vol. 20, no. 3, pp. 696–708, Mar. 2011.

[16] G. Boracchi and A. Foi, "Multiframe raw-data denoising based on block-matching and 3-D filtering for low-light imaging and stabilization," in *The 2008 International Workshop on Local and Non-Local Approximation in Image Processing*, Lausanne, Switzerland, Aug. 2008.

[17] B. Begovic, V. Stankovic, and L. Stankovic, "Contrast enhancement and denoising of Poisson and Gaussian mixture noise for solar images," in *Proc. Int. Conf. Image Process. (ICIP 2011)*, Brussels, Belgium, 11-14 Sep. 2011.

[18] E. Gil-Rodrigo, J. Portilla, D. Miraut, and R. Suarez-Mesa, "Efficient joint Poisson-Gauss restoration using multi-frame $\ell_2$-relaxed-$\ell_0$ analysis-based sparsity," in *Proc. Int. Conf. Image Process. (ICIP 2011)*, Brussels, Belgium, 11-14 Sep. 2011.

[19] A. Chakrabarti and T. Zickler, "Image restoration with signal-dependent camera noise," *CoRR*, vol. abs/1204.2994, 2012.

[20] J. Li, Z. Shen, R. Jin, , and X. Zhang, "A reweighted $\ell_2$ method for image restoration with Poisson and mixed Poisson-Gaussian noise," Tech. Rep., 2012, ftp://ftp.math.ucla.edu/pub/camreport/cam12-84.pdf.

[21] F. Murtagh, J.-L. Starck, and A. Bijaoui, "Image restoration with noise suppression using a multiresolution support," *Astronomy and Astrophysics Supplement*, vol. 112, pp. 179–189, 1995.

[22] A. Foi, "Clipped noisy images: Heteroskedastic modeling and practical denoising," *Signal Process.*, vol. 89, no. 12, pp. 2609–2629, Dec. 2009.

[23] P. L. Combettes and J.-C. Pesquet, "Primal-dual splitting algorithm for solving inclusions with mixtures of composite, Lipschitzian, and parallel-sum type monotone operators," *Set-Valued and Variational Analysis*, vol. 20, no. 2, pp. 307–330, 2012, 10.1007/s11228-011-0191-y.

[24] H. Raguet, J. Fadili, and G. Peyré, "Generalized forward-backward splitting," *SIAM J. Imaging Sci.*, vol. 6, no. 3, pp. 1199–1226, 2013.

[25] L. Condat, "A primal-dual splitting method for convex optimization involving Lipschitzian, proximable and linear composite terms," *J. Optimiz. Theory App.*, vol. 158, no. 2, pp. 460–479, Aug. 2013.

[26] B. C. Vũ, "A splitting algorithm for dual monotone inclusions involving cocoercive operators," *Adv. Comput. Math.*, vol. 38, no. 3, pp. 667–681, 2013.

[27] N. Pustelnik, C. Chaux, and J.-C. Pesquet, "Parallel proximal algorithm for image restoration using hybrid regularization," *IEEE Trans. Image Process.*, vol. 20, no. 9, pp. 2450–2462, Sep. 2011.

[28] G. Demoment, "Image reconstruction and restoration: Overview of common estimation structure and problems," *IEEE Trans. Acous., Speech Signal Process.*, vol. 37, no. 12, pp. 2024–2036, Dec. 1989.

[29] A. Repetti, E. Chouzenoux, and J. Pesquet, "A penalized weighted least squares approach for restoring data corrupted with signal-dependent noise," in *Proc. 20th Eur. Sig. Proc. Conf. (EUSIPCO 2012)*, Bucharest, Roumania, 27-31 Aug. 2012, pp. 1553–1557.

[30] J. J. Moreau, "Proximité et dualité dans un espace hilbertien," *Bull. Soc. Math. France*, vol. 93, pp. 273–299, 1965.

[31] R. T. Rockafellar, "Monotone operators and the proximal point algorithm," *SIAM J. Control Optim.*, vol. 14, no. 5, pp. 877–898, 1976.

[32] H. H. Bauschke and P. L. Combettes, *Convex analysis and monotone operator theory in Hilbert spaces*, Springer, New York, 2011.

[33] M. Elad, P. Milanfar, and R. Rubinstein, "Analysis versus synthesis in signal priors," *Inverse Probl.*, vol. 23, no. 3, pp. 947–968, 2007.

[34] Y. C. Eldar, P. Kuppinger, and H. Bolcskei, "Block-sparse signals: uncertainty relations and efficient recovery," *IEEE Trans. Signal Process.*, vol. 58, no. 6, pp. 3042 –3054, Jun. 2010.

[35] L. I. Rudin, S. Osher, and E. Fatemi, "Nonlinear total variation based noise removal algorithms," *J. Phys. D*, vol. 60, pp. 259–268, 1992.

[36] D. Geman and G. Reynolds, "Constrained restoration and the recovery of discontinuities.," *IEEE Trans. Pattern Anal. Mach. Int.*, vol. 14, no. 3, pp. 367–383, 1992.

[37] S. Lefkimmiatis, A. Bourquard, and M. Unser, "Hessian-based norm regularization for image restoration with biomedical applications," *IEEE Trans. Image Process.*, vol. 21, no. 3, pp. 983–995, Mar. 2012.

[38] P. L. Combettes and J.-C. Pesquet, "A proximal decomposition method for solving convex variational inverse problems," *Inverse Probl.*, vol. 24, no. 6, pp. 065014, Dec. 2008.

[39] L. M. Briceños Arias and P. L. Combettes, "A monotone + skew splitting model for composite monotone inclusions in duality," *SIAM J. Optim.*, vol. 21, no. 4, pp. 1230–1250, Oct. 2011.

[40] P. L. Combettes and J.-C. Pesquet, "Proximal splitting methods in signal processing," in *Fixed-Point Algorithms for Inverse Problems in Science and Engineering*, H. H. Bauschke, R. Burachik, P. L. Combettes, V. Elser, D. R. Luke, and H. Wolkowicz, Eds. Springer-Verlag, New York, 2010.

[41] N. Parikh and S. Boyd, "Proximal algorithms," *Foundations and Trends in Optimization*, vol. 1, no. 3, pp. 123–231, 2013.

[42] P. L. Combettes and V. R. Wajs, "Signal recovery by proximal forward-backward splitting," *Multiscale Model. Simul.*, vol. 4, no. 4, pp. 1168–1200, Nov. 2005.

[43] F. R. Bach, R. Jenatton, J. Mairal, and G. Obozinski, "Optimization with sparsity-inducing penalties.," *Foundations and Trends in Machine Learning*, vol. 4, no. 1, pp. 1–106, 2012.

[44] P. Tseng, "A modified forward-backward splitting method for maximal monotone mappings.," *SIAM J. Control Optim.*, vol. 38, no. 2, pp. 431–446, 2000.

[45] P. L. Lions and B. Mercier, "Splitting algorithms for the sum of two nonlinear operators," *SIAM J. Numer. Anal.*, vol. 16, no. 6, pp. 964–979, 1979.

[46] P. L. Combettes and J.-C. Pesquet, "A Douglas-Rachford splitting approach to nonsmooth convex variational signal recovery," *IEEE J. Selected Topics Signal Process.*, vol. 1, no. 4, pp. 564–574, Dec. 2007.

[47] J.-F. Giovannelli and A. Coulais, "Positive deconvolution for superimposed extended sources and point sources," *Astronomy and astrophysics*, vol. 439, pp. 401–412, 2005.

[48] M. V. Afonso, J. M. Bioucas-Dias, and M. A. T. Figueiredo, "An augmented lagrangian approach to the constrained optimization formulation of imaging inverse problems," *IEEE Trans. Image Process.*, vol. 20, no. 3, pp. 681–695, 2011.

[49] R. I. Boţ and C. Hendrich, "Convergence analysis for a primal-dual monotone + skew splitting algorithm with applications to total variation minimization," *Optimization Online*, 2012.

[50] A. Chambolle and T. Pock, "A first-order primal-dual algorithm for convex problems with applications to imaging.," *Journal of Mathematical Imaging and Vision*, vol. 40, no. 1, pp. 120–145, 2011.

[51] A. Jezierska, C. Chaux, J.-C. Pesquet, H. Talbot, and G. Engler, "An EM approach for time-variant Poisson-Gaussian model parameter estimation," *IEEE Trans. Image Process.*, to appear, 2013, http://hal.archives-ouvertes.fr/hal-00766686.

[52] H. Lantéri and C. Theys, "Restoration of astrophysical images - the case of Poisson data with additive Gaussian noise.," *EURASIP J. Appl. Signal Process.*, vol. 2005, no. 15, pp. 2500–2513, 2005.

[53] T. Fukushima, "Precise and fast computation of Lambert functions without transcendental function evaluations," *J. Comput. Appl. Math.*, vol. 244, no. 0, pp. 77 – 89, 2013.

[54] "The Gene Expression Nervous System Atlas (GENSAT) Project, NINDS contracts N01NS02331 & HHSN271200723701C to The Rockefeller University (New York, NY)," .

[55] F.-X. Dupé, J. M. Fadili, and J.-L. Starck, "A proximal iteration for deconvolving Poisson noisy images using sparse representations," *IEEE Trans. Image Process.*, vol. 18, no. 2, pp. 310–321, Feb. 2009.

[56] X. Bresson, "A short note for nonlocal TV minimization," Tech. Rep., Jun. 2009.

[57] Z. Wang, A. C. Bovik, H. R. Sheikh, and E. P. Simoncelli, "Image quality assessment: from error visibility to structural similarity," *IEEE Trans. Image Process.*, vol. 13, no. 4, pp. 600 –612, Apr. 2004.